Intermetallics 22 (2012) 116–121

Contents lists available at SciVerse ScienceDirect

Intermetallics

journal homepage: www.elsevier.com/locate/intermet

Magnetovolume effects in substituted $Er_{1-x}Gd_xMn_6Sn_6$ intermetallics

Sh. Tabatabai Yazdi [a], N. Tajabor [a,*], M. Rezaee Roknabadi [a], M. Behdani [a], F. Pourarian [b]

[a] Department of Physics, Faculty of Sciences, Ferdowsi University of Mashhad, Mashhad 91775-1436, Iran
[b] Department of Materials Science & Engineering, Carnegie Mellon University, Pittsburgh, PA 15213, USA

ARTICLE INFO

Article history:
Received 20 June 2011
Received in revised form
2 August 2011
Accepted 4 August 2011
Available online xxx

Keywords:
A. Rare-earth intermetallics
B. Magnetic properties

ABSTRACT

The thermal expansion and spontaneous magnetostriction of polycrystalline samples of $Er_{1-x}Gd_xMn_6Sn_6$ ($0 \le x \le 1$) intermetallics with hexagonal $HfFe_6Ge_6$-type structure are investigated in the temperature range of 77–520 K. The Gd substitution has significant effect on the interatomic distances and especially on inter-sublattice R–Mn couplings. The replacement of Er by Gd causes the lattice constants to increase due to the larger atomic radius of Gd compared with Er. It also results in increasing the ordering temperature as well as the spontaneous magnetostriction values following reinforcement the R–Mn coupling. The examined samples exhibit considerable thermal expansion anomalies at the Néel temperature ($T_N = 340$ and 335 K for the samples with $x = 0$ and 0.2, respectively) and also at $T_M = 309$–311 K where the Mn moments experience collapse-like reduction. Whereas, trivial anomalies are revealed at the Curie points ($T_C = 77$ K for the sample with $x = 0$, 164 and 383 K for $x = 0.2$, 419 and 434 K for $x = 0.6$ and 1, respectively). From the results, it is concluded that the magnetovolume effects in these compounds originate mainly from the antiferromagnetic interlayer Mn–Mn exchange interactions, and the intraplane ferromagnetism does not influence the magnetoelasticity.

1. Introduction

The ternary intermetallic compounds containing rare-earth R, transition metal T and a p-group element X have attracted considerable attention due to their interesting magnetic properties. Among them, a great number of publications have been devoted to RMn_6Sn_6 compounds (with R = Sc, Y, Gd–Tm and Lu), including magnetization measurements [1–3], neutron diffraction [4], Mössbauer spectroscopy [4], NMR spectroscopy [5], transport, magnetotransport [6], magneto-optical measurements [7], and some theoretical studies on their electronic structure [8]. All these compounds crystallize in the hexagonal $HfFe_6Ge_6$-type structure with space group P6/mmm (Fig. 1). This crystal structure can be described as layers of R and Mn atoms alternately stacked along the *c*-axis in the sequence Mn–(R,Sn)–Mn–Sn–Sn–Sn–Mn. The magnetic structure of RMn_6Sn_6 compounds consists of two interacting subsystems: one of them is composed of R atoms and Mn atoms form the other. The observed complex magnetic behavior of these compounds with various magnetic phase transitions originates from the temperature-dependent competition between the Mn–Mn, R–Mn and R–R interactions as well as the magnetocrystalline anisotropies of the R and Mn sublattices. Both the intralayer Mn–Mn interaction (J_0) which is the strongest, and the interlayer Mn–Mn exchange interaction through the Mn–Sn–Sn–Sn–Mn slab (J_1) are always positive (ferromagnetic), while the nature of that within the Mn–(R,Sn)–Mn slab (J_2) depends on the Mn–Mn interatomic distances and so is very sensitive to the R element [9,10]. The R–Mn coupling is negative for heavy R elements and strongest for R≡Gd [11,12], with the same order of magnitude as the interlayer Mn–Mn one. Among the RMn_6Sn_6 family, the compound with R≡Er has a complex behavior displaying several transitions: spontaneous (temperature-induced) transitions characterized by antiferromagnetism below $T_N = 352$ K and a transition to ferrimagnetic state at about 75 K, as well as metamagnetic (field-induced) ones in its ordered state [1]. In order to better understand the contributions from the two sublattices to these magnetic behaviors, we decided to study the effect of Gd substitution for Er on the structure and certain magnetic and magnetoelastic properties of $Er_{1-x}Gd_xMn_6Sn_6$ ($0 \le x \le 1$) compounds. Since the Mn sublattice favors an easy plane anisotropy and Er and Gd both reveal an easy plane behavior in the whole ordered state [4] as well, there will be no competition between the two sublattice anisotropies and consequently no spin reorientation process is expected in the studied compounds. Because of the strong interatomic distance dependence of the Mn–Mn interlayer interactions, one may expect that these magnetic transitions involving variation of arrangement of Mn moments, are likely to be accompanied by anomalies in the magnetoelastic behaviors.

* Corresponding author. Tel.: +98 511 8817741; fax: +98 511 8763647.
E-mail addresses: tajabor@ferdowsi.um.ac.ir, ntajabor@yahoo.com (N. Tajabor).

0966-9795/$ – see front matter © 2011 Published by Elsevier Ltd.
doi:10.1016/j.intermet.2011.08.002

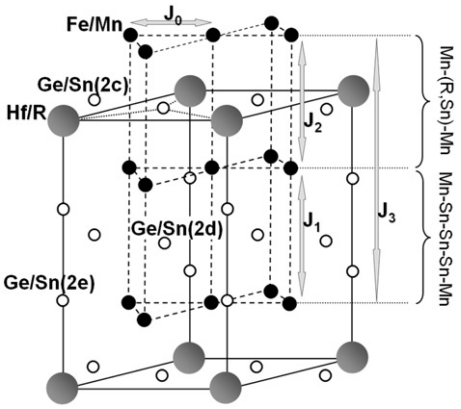

Fig. 1. Schematic representation of the $HfFe_6Ge_6$-type crystal structure and magnetic interactions in RMn_6Sn_6 compounds.

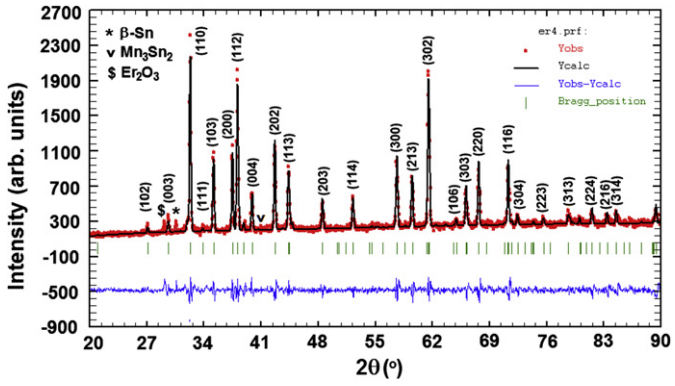

Fig. 2. Observed (circles) and calculated (solid lines) XRD pattern of the $Er_{0.4}Gd_{0.6}Mn_6Sn_6$ sample at room temperature. The vertical bars indicate the position of Bragg reflections. The difference between the observed and calculated intensities is given at the bottom of the diagram. The pattern has been indexed on the basis of the $HfFe_6Ge_6$-type structure.

Therefore, in the present work, we have investigated the effect of Gd substitution for Er on the thermal expansion and spontaneous magnetostriction of $Er_{1-x}Gd_xMn_6Sn_6$ ($0 \le x \le 1$) compounds.

2. Experiments

The $Er_{1-x}Gd_xMn_6Sn_6$ ($0 \le x \le 1$) polycrystalline samples were prepared by arc melting the constituent elements under high-purity argon atmosphere in a water-cooled copper hearth. The raw materials used were at least of 99.9% purity. The ingots were turned over and remelted several times to insure their homogeneity. The synthesized ingots wrapped in a tantalum foil were sealed in an evacuated quartz tube, annealed at 1023 K for 4 weeks, and then quenched in water to obtain single-phase materials. The purity and microstructure of the prepared samples were checked using X-ray powder diffraction (XRD) with monochromatic Cu Kα radiation ($\lambda \sim 1.5406$ Å) in the 2θ range of 20–90° in a continuous scan mode with a step width of 0.05° and using a scanning electron microscopy (SEM) (Leo 1450VP, Carl Zeiss SMT, Germany). For structural characterization, analysis of the obtained XRD profiles were performed using the Rietveld refinement method, through the Fullprof software (see for instance [13]). In order to reveal the magnetic phase transitions, the thermomagnetic measurements were carried out using a LakeShore 7000 magneto-susceptometer with an ac magnetic field of 50 A/m peak value at 125 Hz in the temperature range of 77–330 K. The linear thermal expansions TE normalized to 77 K ($\Delta l/l = (l_T - l_{77K})/l_{77K}$) were measured using the strain-gage Wheatstone bridge technique on disk-shaped samples with a diameter of about 6 mm and thickness of about 2 mm in the temperature range of 77–520 K. The accuracy of these measurements was better than 2×10^{-6}.

3. Results and discussion

The XRD patterns indicate that the samples are highly pure single-phase with $HfFe_6Ge_6$-type structure (S.G. P6/mmm) with small amounts of β-Sn, R_2O_3 and Mn_3Sn_2. The presence of such minor impurity phases has been reported in most previous attempts to prepare RMn_6Sn_6 samples by arc-melting or solid-state reaction method, for instance ref. [14,15]. Fig. 2 presents, as an example, the fitted diffraction pattern for $Er_{0.4}Gd_{0.6}Mn_6Sn_6$ sample at room temperature. The refined crystallographic parameters including lattice parameters and the conventional agreement factors of the Rietveld analysis are summarized in Table 1. The lattice parameters obtained for the two end members of the present series are well close to the reported values in literature [16]. The variation of the lattice parameters and the corresponding unit cell volume versus Gd content (x) are depicted in Fig. 3. As readily seen, the replacement of Er by Gd causes the lattice constants to increase; this is related to the larger atomic radius of Gd compared with Er. The non-linear variation of cell volume suggests that this system does not follow the Vegard's law; the lattice expands far more rapidly than Vegard's law predicts. It is worth noting that the c/a ratio remains approximately constant indicating an isotropic variation of the lattice. This should be due to the relatively similar electronic configurations and ionic radii of Er and Gd. The SEM microstructural analysis shows that the prepared samples contain mainly grains of 1:6:6 phase with the mean size of about 200 micron and minor impurity phases in grain boundaries, consistent with the XRD results.

The ac magnetic susceptibility χ_{ac} of $Er_{1-x}Gd_xMn_6Sn_6$ ($x = 0$ and 0.2) samples under a zero dc magnetic field in the temperature range of 77–330 K are presented in Fig. 4. The χ_{ac} measurements of samples with $x = 0.6$ and 1 (not presented here) are characterized by a non-linear increase without revealing any transition point in the studied temperature range. This is in agreement with the reported neutron diffraction and magnetization measurements for $GdMn_6Sn_6$ [4] and originates from the strong Mn–Gd antiferromagnetic interaction causing the simultaneous ordering of the two sublattices and consequently a ferrimagnetic arrangement for the two compounds with a high Gd content ($x \ge 0.6$). The thermomagnetic curve for the sample with $x = 0.2$ (Fig. 4) reveals a peak at about $T_{C1} = 165$ K corresponding to its magnetic transition point. The observed behavior can be explained as follows: at temperatures below T_{C1}, the strong R–Mn antiferromagnetic interaction which as said, is very sensitive to the Mn–Mn interatomic distances, dominates the Mn–Mn one and causes the R and Mn sublattices to order simultaneously leading to a ferrimagnetic arrangement. At higher temperatures, as the R–Mn interaction

Table 1
Rietveld refined crystallographic parameters of $Er_{1-x}Gd_xMn_6Sn_6$ samples.

Gd content (x)	a (Å)	c (Å)	V (Å^3)	c/a	R_p(%)	R_{wp}(%)	R_{exp}(%)	χ^2
0	5.52743	9.02036	238.671	1.6319	7.56	10.2	5.71	3.16
0.2	5.52835	9.01982	238.736	1.6316	7.26	9.94	5.70	3.10
0.6	5.53266	9.02602	239.274	1.6314	8.55	11.9	5.86	4.12
1	5.54671	9.04348	240.956	1.6304	7.38	11.4	5.82	3.85

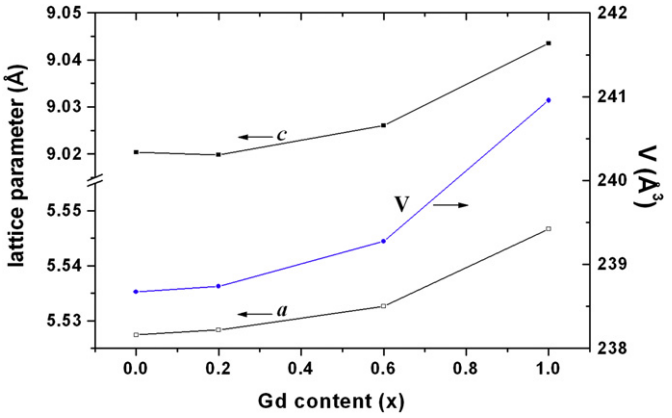

Fig. 3. Variation of crystal structure parameters a and c and the corresponding unit cell volume versus Gd content (x) in $Er_{1-x}Gd_xMn_6Sn_6$ samples ($0 \le x \le 1$).

weakens due to thermal expansion, the Mn–Mn one dominates resulting in an antiferromagnetic state. The χ_{ac} behavior of the $x = 0$ sample (Fig. 4) is characterized by a strong increase of magnetization at low temperature, without displaying the exact ordering point. However, the transition temperature is obtained from its first derivative curve. This behavior was expected and can be understood based on the above discussion: at low temperature, the Er–Mn strong antiferromagnetic coupling causes the Er and Mn sublattices to order ferromagnetically in the (001) plane resulting in a collinear ferrimagnetic order [4]. Hence, the $T_C = 77$ K ordering point may be attributed to the ordering of the Er sublattice. As temperature increases and the Er–Mn interaction weakens, Mn–Mn coupling dominates. Therefore, the Mn sublattice orders antiferromagnetically and the Er sublattice is in a paramagnetic state, resulting in an antiferromagnetic ordering between 77 and above 330 K (330 K was the highest available temperature in this measurement) It can also be seen from Fig. 4 that a distinct feature appears at about 160 K. The first possible origin of this anomaly may be the presence of some magnetic impurity phase in the sample. However, this is less likely because a secondary phase with such a pronounced peak would have been detected easily in the XRD pattern of the sample (the magnetic transition temperatures of the detected minor phases do not correspond to this point: β-Sn is a paramagnetic, Er_2O_3 has a transition at $T_N = 3.4$ K and Mn_3Sn_2 at $T_{C1} = 262$ and $T_{C2} = 227$ K). This not being the case, we can conclude that it is a feature belonging to the main phase needing further investigation. The insignificant distinct feature at about 260 K in the thermomagnetic curves of all the samples should be due to the minor impurity phase Mn_3Sn_2.

Fig. 5 shows the temperature dependence of the zero-field linear thermal expansion dl/l of $Er_{1-x}Gd_xMn_6Sn_6$ ($0 \le x \le 1$) samples in the range of 77–520 K. The LTE coefficients (α) versus temperature depicted by taking a point-to-point temperature derivative of the dl/l data are presented in Fig. 5, as well. All the curves display a metallic behavior with a change of slope at a point which is more readily observed as anomalies in the $\alpha(T)$ behavior.

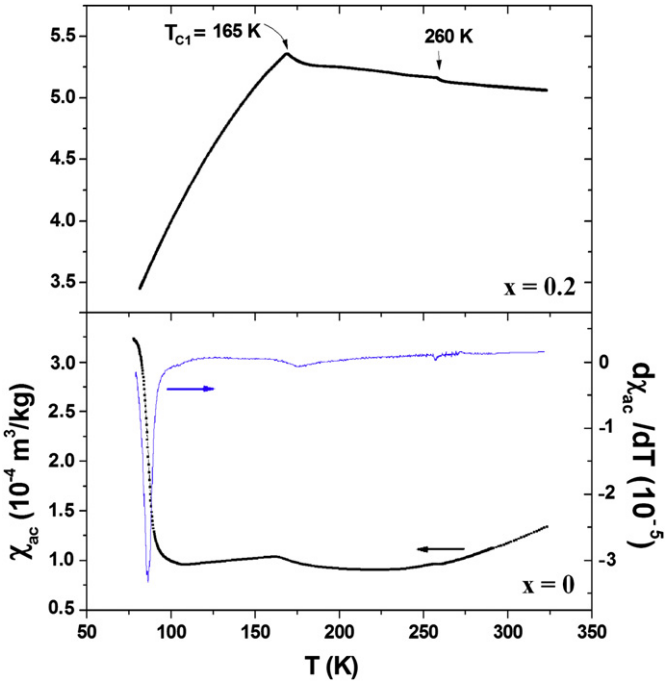

Fig. 4. Temperature dependence of the ac susceptibility χ_{ac} of the $Er_{1-x}Gd_xMn_6Sn_6$ samples with $x = 0$ and 0.2 with an ac magnetic field of 50 A/m peak value at 125 Hz and in zero dc magnetic field.

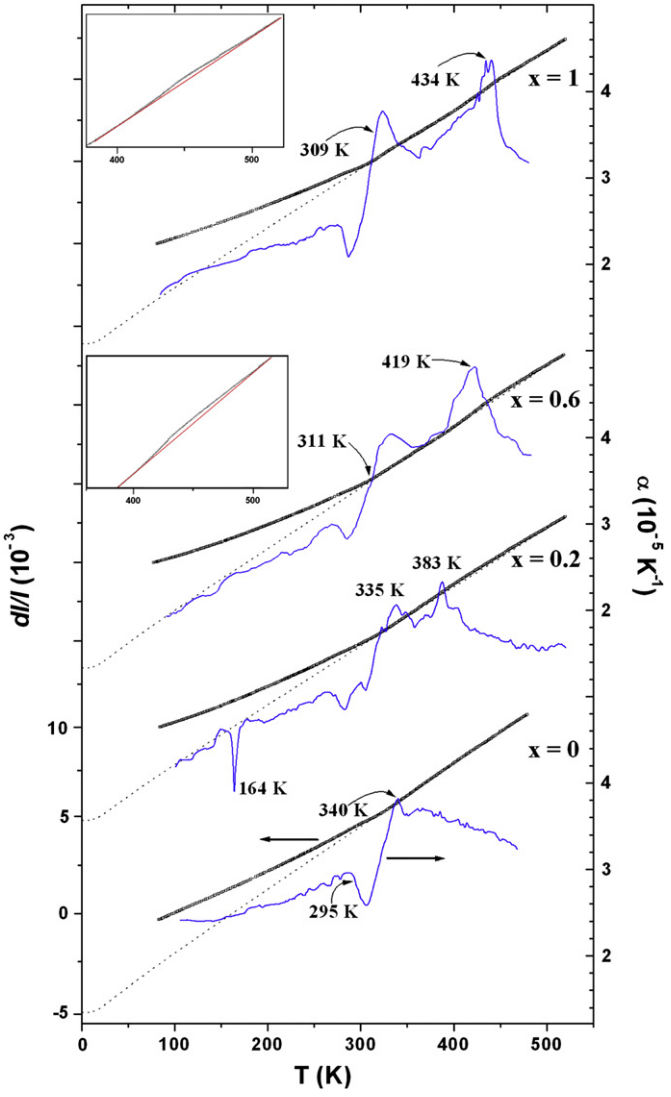

Fig. 5. Temperature dependence of the linear thermal expansion (LTE) and thermal expansion coefficient α versus temperature for $Er_{1-x}Gd_xMn_6Sn_6$ ($0 \le x \le 1$) samples. The dashed lines show the simulated phonon contribution (Grüneisen law) using $\theta_D = 102$ K.

The effect of Gd substitution is revealed to be an increase in the α values attributed to the ionic size. It is worth mentioning that for all the samples, the slope change at transition temperatures is continuous and well-defined indicating second order phase transitions (no first order structural transition occurring). For the sample with $x = 0$, this anomalous behavior of LTE coefficient extends over the temperature interval of 295–340 K, namely from the onset of the antiferromagnetic–paramagnetic transition to the point where this phenomenon is completed. The observed significant volume expansion at about 340 K should be due to a transition of the Mn sublattice to the antiferromagnetic order. It is believed and also confirmed by the present χ_{ac} measurements, that at about 77 K, the Er sublattice moments in $ErMn_6Sn_6$ align ferromagnetically, but as seen this alignment does not cause any notable anomaly in the thermal expansion behavior. These observations and the above discussion indicate a $T_N = 340$ K and $T_C \approx 77$ K for the $ErMn_6Sn_6$ sample, close to the 352 and 75 K values suggested by Venturini et al. [1]. For the sample with $x = 0.2$, in addition to considerable expansion accompanying the transition from antiferromagnetic to ferrimagnetic (at about $T_N = 335$ K), the $\alpha(T)$ behavior reveals anomalies at 164 K, where the ac susceptibility has an anomaly (point at which the R sublattice orders) and at 383 K, too. This can be interpreted as follows: as mentioned, the R–Mn coupling is proportional to $J_{R-Mn}M_RM_{Mn}$ (J is the exchange coupling parameter and M is the saturation magnetization), which in turn is proportional to $(g-1)\langle J\rangle_R M_{Mn}$ (g factor of the R component) [11]. The quantity $(g-1)J$ is the largest for R = Gd and falls off rapidly toward both ends of the lanthanide series ($J_{Gd-Mn} = -0.93$ meV and $g = 2$ [12]). Therefore, Gd substitution makes the R–Mn coupling stronger leading to transition from antiferro- to ferrimagnetic state at about $T_N = 335$ K. Hence, the antiferromagnetic state is not stable and as temperature increases, thermal expansion causes the Mn–Mn interlayer interaction, which is sensitive to the interatomic distances, to turn into positive and the system reenters the ferrimagnetic state before becoming paramagnetic at about 383 K. Upon Gd substitution, the interatomic distances increase and consequently the Mn–Mn coupling weakens. However, as seen from Fig. 3, introduction of 20% Gd in $ErMn_6Sn_6$ does not greatly change the cell parameters and volume. So the Mn–Mn interactions should not significantly differ, and therefore the T_N of the two compounds with $x = 0$ and 0.2 vary slightly.

For the compounds with higher Gd concentration ($x \geq 0.6$), LTE behavior displays a shallow anomaly near T_C ($T_C = 419$ and 434 K for the samples with $x = 0.6$ and 1, respectively) which is highlighted in the $\alpha(T)$ curves, along with a change of slope at a $T_M = 309$–311 K. The occurrence of the observed positive volume anomalous behavior upon the ferri- to paramagnetic transition can be explained as follows: the loss of ferrimagnetism on heating through T_C leads to a decrease in the number of nearest R–Mn neighbors with the indirect 4f-5d-3d exchange interactions with antiparallel spins (and therefore attraction interaction) and hence the crystal volume increases. The anomalous behavior (noticeable volume expansion) observed around T_M, should be due to the collapse-like reduction of ferromagnetic Mn moments at this temperature, consistent with the thermal variation of Mn moments in this compound reported previously [4]. This has been discussed in detail in our previous paper on $GdMn_6Sn_6$ sample [17]. In compounds with lower Gd content ($x \leq 0.2$), the anomalous behavior associated with the Mn moments reduction coincides somewhat and should be overshadowed by the magnetovolume effect due to the magnetic transitions resulting from sign reversal of the R–Mn interactions.

In summary, the examined samples exhibit considerable TE anomalies (notable volume expansion) at the T_N of the related sample and also at $T_M = 309$–311 K where the Mn moments experience collapse-like reduction, while trivial anomalies are revealed at the T_C points. In regard of magnetic arrangements of sublattices at the transition temperatures of the involved samples, one can conclude that the magnetovolume effects in these compounds originate mainly from the antiferromagnetic interlayer Mn–Mn exchange interactions, and the intraplane ferromagnetism does not influence the magnetoelasticity.

The values of the transition temperatures of the studied samples estimated from the α curves are summarized in Table 2, which for the two end members of the series ($x = 0$ and 1) are well consistent with the literature [1]. As seen, the ordering temperature increases by the Gd content, although one may expect otherwise from the increase in the unit cell parameters by Gd substitution. This is an important difference between the magnetic behaviors of stannides and germanides; in RMn_6Ge_6 compounds, the ordering temperature decreases with the size of the R element due to the larger Mn–Mn interatomic distances and consequently weaker Mn–Mn interactions [18]. An increase in the size of the R element acts in an opposite way in RMn_6Sn_6 compounds [1]. In stannides, ordering temperature increases with an almost linear trend with respect to the ionic radius of R element, except for those with nonmagnetic R and Tm. This can be explained using the two-sublattice mean field model [19] expressing T_C in terms of R–Mn and Mn–Mn coupling constants (J_{R-T} and J_{T-T}). As mentioned above, in RMn_6Sn_6 compounds there are several interactions: a positive interalayer Mn–Mn direct interaction (J_0), a positive interlayer Mn–Mn superexchange interaction through Mn–Sn–Sn–Sn–Mn slab (J_1), an interatomic distance-dependent interlayer Mn–Mn superexchange through Mn–(R,Sn)–Mn slab (J_2) and a next nearest layer long-range interaction (J_3). The different observed magnetic arrangements arise from the competition between J_2 and J_3, and in compounds with heavy R elements, with J_{R-Mn}. In the case of the compound with R≡Gd owing to the negative $J_{R\text{-}Mn}$ with the highest value, positive J_2 (for larger Mn–Mn distances) and negative J_3 may be somewhat compensated and hence, J_{Gd-Mn} being preponderant tends to align the Mn moments within the Mn–(R,Sn)–Mn slab. Therefore, Gd introduction causes the ordering temperature to increase.

The magnetic contribution to the thermal expansion $(dl/l)_m$ can be estimated from the difference between the observed dl/l curve and the usual anharmonic phonon contribution governed by the Grüneisen law. According to this empirical law $\alpha(T) = \gamma \kappa_T C_v(T)/3$, where the Grüneisen parameter γ and isothermal compressibility coefficient κ_T are relatively insensitive to temperature, the TE coefficient α and specific heat C_v have essentially a linear relationship. Since contribution from the electronic subsystem is negligible in comparison with the magnetic and lattice ones, the difference between the observed TE and the phonon one which we use in Debye's elementary model with $\theta_D = 102$ K derived from the specific heat data [20], is due to the magnetic interactions. The calculated nonmagnetic contribution that has been fitted to the experimental results in the paramagnetic regime is depicted in Fig. 5 as a dashed line. Assuming that the linear thermal expansion dl/l is isotropic, the spontaneous volume magnetostriction is $\omega_s = 3(dl/l)_m$. The temperature dependence of the ω_s values of

Table 2
Magnetic transition temperatures of $Er_{1-x}Gd_xMn_6Sn_6$ samples (Fi≡ferrimagnetic, AF≡antiferromagnetic).

Gd content (x)	T_{C1} (K)	T_N (K)	T_C (K)	Magnetic order
0	≈77	340	–	Fi-AF
0.2	164	335	383	Fi-AF-Fi
0.6	–	–	419	Fi
1	–	–	434	Fi

$Er_{1-x}Gd_xMn_6Sn_6$ ($0 \le x \le 1$) samples are shown in Fig. 6. As seen, in all samples, ω_s does not vanish at the ordering point and, as in several related intermetallics, some insignificant spontaneous magnetostriction effects do persist at higher temperatures in the paramagnetic phase. This reflects existence of short-range magnetic correlations above the ordering temperature. As is one's expectation from the strong Gd–Mn interaction, Gd substitution reduces the temperature interval where the short-range orders exist, indicating stabilization of the magnetic state.

Fig. 6 reveals that ω_s values of the studied samples increase slightly by Gd substitution. In order to analyze in more detail the observed spontaneous magnetovolume effects, let us consider a phenomenological theory stating that the extra contribution to the thermal expansion over the lattice one is caused by a change in the magnitude of local moments and also by a change in the relative orientations of the neighboring ones [21]. It means that magnetic volume change is composed of two contributions: a band term being proportional to the square amplitude of the local spin fluctuations or in other words, the square of the local moments (longitudinal spin fluctuations or Stoner excitations [22]) and an interaction term being proportional to the pair correlation function between local moments (transverse spin fluctuations or spin-wave excitations). Therefore, the magnitude and temperature dependence of ω_s of these intermetallics in a two-sublattice model can be described as follows [23]:

$$\omega_s = n_{\mathrm{Mn-Mn}}\mu_{\mathrm{Mn}}^2 + n_{\mathrm{Mn-}R}\mu_{\mathrm{Mn}}\mu_R + n_{R-R}\mu_R^2 \quad (1)$$

where $n_{\mathrm{Mn\text{-}Mn}}$ and $n_{\mathrm{R-R}}$ are the magnetoelastic-coupling coefficients in the Mn and R sublattices, respectively, and $n_{\mathrm{Mn-R}}$ is the inter-sublattice coupling coefficient ($n_{3d-3d} >> n_{3d-4f} >> n_{4f-4f}$). The last term is known to be negligible in intermetallics with a high 3d metal content [24]. In the involved compounds, the average moments of Mn atoms are almost constant, while the R atoms one differs in each sample (in low temperatures $\mu_{Gd} < \mu_{Er}$ [4]). Therefore, trivial increase in ω_s values of $Er_{1-x}Gd_xMn_6Sn_6$ compounds by Gd substitution (see Fig. 6) indicates the predominant influence of strong Gd–Mn coupling.

Resuming this paper, from the low values of ω_s in the T_C regions, we conclude that the transverse spin fluctuations of R magnetic moments are the main origin of volume effects in these regions, whereas, the large ω_s values at T_N and T_M regions can be ascribed to the longitudinal spin fluctuations. Inspecting again the Mn moment collapse at T_M, it should be mentioned that, considering a linear relation between $n_{\mathrm{Mn-Mn}}$ and the unit cell dimensions [25], a volume change of more than 10% would be expected if the Mn moment of 2.4 μ_B (at temperatures below 300 K) collapsed completely at T_M. The observed value of about 1% suggests that the Mn moment does not collapse to zero at T_M, but remains finite due to spin fluctuations.

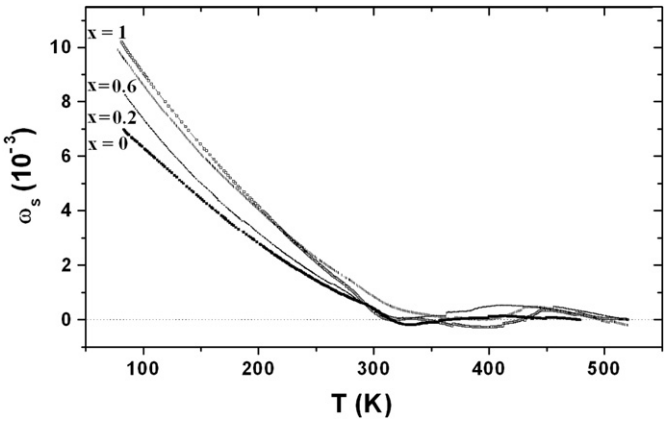

Fig. 6. Temperature dependence of the spontaneous volume magnetostriction ω_s for $Er_{1-x}Gd_xMn_6Sn_6$ ($0 \le x \le 1$) samples.

4. Conclusions

The highly pure single-phase polycrystalline samples of $Er_{1-x}Gd_xMn_6Sn_6$ ($0 \le x \le 1$) intermetallics were prepared by arc melting method. All the compounds are isotypic and possess a hexagonal $HfFe_6Ge_6$-type structure (S.G. P6/mmm). The replacement of Er by Gd causes the lattice constants to increase; this is related to the larger atomic radius of Gd compared with Er. The Gd substitution has significant effect on the interatomic distances and especially on inter-sublattice R–Mn couplings. Hence, the substituted $Er_{1-x}Gd_xMn_6Sn_6$ compounds display abundant behaviors. In the present paper, we have reported the results of linear thermal expansion of the involved samples in the temperature range of 77–520 K measured using the strain-gage technique. The experimental results obtained are discussed in the framework of two-magnetic sublattice by bearing in mind the lattice parameter dependence of interlayer Mn–Mn exchange interactions in these layered compounds. The studied samples exhibit considerable TE anomalies (notable volume expansion) at T_N of the related sample (340 and 335 K for the samples with $x = 0$ and 0.2, respectively) and also at T_M = 309–311 K where the Mn moments experience collapse-like reduction. Whereas trivial anomalies are revealed at T_C points (77 K for the sample with $x = 0$, 164 and 383 K for $x = 0.2$, 419 and 434 K for $x = 0.6$ and 1, respectively). Consequently, the magnetovolume effects in these compounds originate mainly from the antiferromagnetic interlayer Mn–Mn exchange interactions, and the intraplane ferromagnetism does not influence the magnetoelasticity. The transition temperature values of the samples estimated from the α curves show that Gd substitution increases the ordering temperature following the reinforcing of the R–Mn coupling.

The computed spontaneous volume magnetostriction (ω_s) values of the studied samples reveal a trivial increase on Gd substitution indicating the predominant influence of strong Gd–Mn coupling in the magnetovolume effects of these compounds. The last remark is that Gd substitution reduces the temperature interval where the short-range orders exist in the paramagnetic phase, indicating stabilization of the magnetic state.

References

[1] Venturini G, Chafik El Idrissi B, Malaman B. J Magn Magn Matter 1991;94:35.
[2] Clatterbuck DM, Gschneidner Jr KA. J Magn Magn Matter 1999;207:78.
[3] Suga K, Kindo K, Zhang L, Brück E, Buschow KHJ, de Boer FR, et al. J Alloys Compd 2006;408–412:158.
[4] Malaman B, Venturini G, Welter R, Sanchez JP, Vulliet P, Ressouche E, et al. Magn Mater 1999;202:519.
[5] Shimizu K, Hori T. J Magn Magn Mater 2007;310:1874.
[6] Yao Jin-lei, Zhang Shao-ying, Liu Bao-dan, Shen Bao-gen, Wang Ru-wu, Zhang Li-gang, Yang De-ren, Yan Mi. J Appl Phys 2004;95:7061.
[7] Clatterbuck DM, Lange RJ, Gschneidner Jr KA. J Magn Magn Mater 1999;195:639.
[8] Mazet T, Tobola J, Venturini G, Malaman B. Phys Rev B 2002;65(104406):1.
[9] (a) Canepa F, Duraj R, Lefèvre C, Malaman B, Mar A, Mazet T, et al. J Alloys Compd 2004;383:10;
(b) Brabers JHVJ, Nolten AJ, Kayzel F, Lenczowski SHJ, Buschow KHJ, de Boer FR. Phys Rev B 1994;50(22):16410.
[10] Mazet T, Walter R, Malaman B. J Alloys Compd 1999;284:54.
[11] Brabers JHVJ, Dujin VHM, de Boer FR, Buschow KHJ. J Alloys Compd 1993;198:127.
[12] Tils P, Loewenhaupt M, Buschow KHJ, Eccleston RS. J Alloys Compd 1998;279:123.
[13] Roisnel T, Rodríguez-Carvajal J. Mater Sci Forum 2001;378–381:118.
[14] Cakir O, Dincer I, Elmali A, Elerman Y, Ehrenberg H, Fuess H. J Alloys Compd 2006;416:31.
[15] Venturini G. J Alloys Compd 2005;400:37.

[16] Lian Zhang, PhD thesis, Universiteit van Amsterdam (2005).
[17] Tabatabai Yazdi Sh, Tajabor N, Behdani M, Rezaee Roknabadi M, Sanavi Khoshnoud D, Pourarian F. J Magn Magn Mater 2011;323:2070.
[18] Venturini G, Welter R, Malaman B. J Alloys Compd 1992;185:99.
[19] Buschow KHJ. Rep Prog Phys 1991;54:1123.
[20] Duijn H.G.M, PhD thesis, Universiteit van Amsterdam (2000) p 141.
[21] Shiga M, Phys J. Soc Jpn 1981;50:2573.
[22] Algarabel PA, Ibarra MR, Marquina C, Yuasa S, Miyajima H, Otani y. J Appl Phys 1996;79:4659.
[23] Lee EW, Pourarian F. Phys Status Solidi (a) 1976;33:483.
[24] Andreev AV. In: Buschow KHJ, editor. Handbook of magnetic materials, vol. 8; 1995. p. 59. North-Holland, Amsterdam.
[25] Brabers JHVJ, de Groot CH, Buschow KHJ, de Boer FR. J Magn Magn Mater 1996;157/158:639.